Proceedings of the Australian Combustion Symposium
November 6-8, 2013, The University of Western Australia

Recent Progress in Modeling Reacting Diesel Sprays

John Abraham[1, 2]
[1] School of Mechanical Engineering, Purdue University, West Lafayette, IN 47907-2088, USA
[2]School of Mechanical Engineering, University of Adelaide, Adelaide, South Australia 5005, Australia

Abstract

This paper will begin by discussing the structure of non-reacting and reacting diesel sprays. Results from recent work employing RANS to model the non-reacting spray will be presented. It will be shown through detailed comparison with measured results that under conventional high-pressure high-temperature chamber and high-pressure injection conditions, the vaporizing diesel spray behaves like a gas jet. Several turbulence-chemistry interaction models for the reacting diesel spray will be reviewed. RANS simulation results of reacting diesel sprays in which an unsteady flamelet progress variable (UFPV) model is employed for turbulence/chemistry interactions will be discussed in detail. It is shown that the model can predict ignition delay and flame lift-off heights with reasonable accuracy. The model has also been extended to model nitrogen oxides and soot distribution in the reacting diesel sprays. Nitrogen oxides are modeled using the mechanism from Gri-Mech 3.0 and soot is modeled using a kinetic mechanism coupled with a tracer particle approach to estimate residence times within the jet. Initial simulations of the reacting diesel jet using a large-eddy simulation approach coupled with a UFPV model will also be presented. Areas for further work in modeling diesel sprays will be discussed.

Keywords: diesel engines, transient diesel sprays, diesel spray modeling, transient jets, reacting diesel sprays

1. Introduction

Diesel engines have been the focus of extensive experimental and computational investigations during the last 20 years with the primary driver being regulatory pressure to reduce exhaust emissions. It is interesting to recall that the spark-ignition (SI) engine was the subject of much research in the 1960s and 70s because of similar pressure on exhaust emissions. In the case of the SI engine the problem was ultimately addressed by the three-way catalytic converter which reduced pollutants from conventional SI engines to very low and acceptable values although research on advanced SI combustion systems, e.g. direct-injection spark-ignition (DISI) engines continues. Following a similar path, diesel engine manufacturers worldwide are adopting exhaust aftertreatment as the immediate solution to control exhaust emissions of particulate matter (PM) and nitrogen oxides (NO_x). These aftertreatment devices, unlike the three-way catalytic converter of the SI engine, are bulky and expensive and reducing their size and cost is imperative. This can be achieved by reducing exhaust emissions through in-cylinder combustion and injection system modifications. Furthermore, optimizing the performance of the aftertreatment devices requires a clear understanding of the emissions characteristics. Whether the effort is directed toward reducing emissions or optimizing aftertreatment devices, modeling of the transient sprays, in-cylinder fluid flow, and chemical kinetics of pollutant formation are critical in achieving the goals. The accuracy of the models is dependent on the understanding of the processes involved. The objective of this paper is to review the current status of this understanding and the progress that has been made in modeling the diesel spray.

Injection in direct-injection (DI) diesel engines is into a chamber where the temperature is in the range of 800-1200 K and the pressure is 4-10 MPa prior to combustion. Injection pressures vary from 150250 MPa. Injection at these pressures generates injection velocities in the range of 500-750 m/s. Under these conditions, the liquid is atomized to drops whose diameters lie in the range of 1-10 microns [1-7]. Solid-cone sprays are the norm in diesel engines. In addition to primary breakup of the liquid during atomization, the ligaments and drops which are formed as a result of primary breakup undergo drop-drop interactions and secondary breakup in the near-field of the spray. There has been discussion in the literature on the existence of an intake liquid core in the spray though no firm conclusions have been reached [1, 8-10]. The near-field of the spray where the liquid-phase length reaches its maximum length achieves a statistical steady-state in a relatively short period of time (0.1-0.3 ms). Note that measurements in the dense atomizing region of the spray are difficult and so drop sizes in this region have to be deduced from measurements at the periphery of the spray or from measurements in the dilute spray several hundred diameters downstream of the orifice. This deduction often involves the use of spray models in which drop sizes are estimated from models in the atomization region and then matched to those measured downstream. This is a difficult task prone to errors because of inadequate understanding of atomization and drop-interaction sub-models as reflected in a wide range of proposed sub-models and numerical inaccuracies in modeling the sprays [1-2, 9, 11-19].

The drops generated during atomization transfer momentum to the chamber gas, entrain the gas, and

* Corresponding author:
Email: jabraham@purdue.edu; john.abraham@adelaide.edu.au

undergo rapid vaporization. The jet penetrates as a vapor jet beyond the maximum length to which the drops penetrate, i.e. the liquid-phase length – this length can extend up to 2-3 cm in conventional diesel sprays [15, 20-22]. While the physics of atomization and the structure of the spray in the atomizing region are not well understood, the quasi-steady structure of the spray downstream of the maximum liquid-phase length has been fairly well-characterized through extensive experimental studies – in fact, it behaves like a gas jet [13-15, 20, 23-24]. Figure 1 shows a schematic of the high-pressure diesel spray. Though not indicated as such in the schematic, the spray angle in the near-field of the jet is generally smaller than in the far-field [1, 20, 25-26]. In the far-field the spreading angle approaches that of the turbulent gas jet. Identified in Figure 1 are the intact liquid core (L_1), the liquid-phase penetration length (L_2), a quasi-steady region of the jet (L_3), and the transient head-vortex (L_4).

In the case of engine sprays, where the injection is intermittent, it is important to consider the transient nature of the spray in trying to understand mixing. In Fig. 1, this transient behavior is predominant in the head-vortex. Note, however, that for a period of time after start of injection the part of the spray where transient mixing and development are important constitutes a significant fraction of the spray. The dynamics of the starting jet during the early stages of injection are still the subject of experimental and computational inquiry [24, 27-31]. To the author's best knowledge, there has been no study specific to diesel sprays. When injection ends, the behavior of the jets is again influenced strongly by transients in the trailing part of the jet. In fact, these transients can influence the mixing behavior in diesel engines and impact pollutant emissions [32-33].

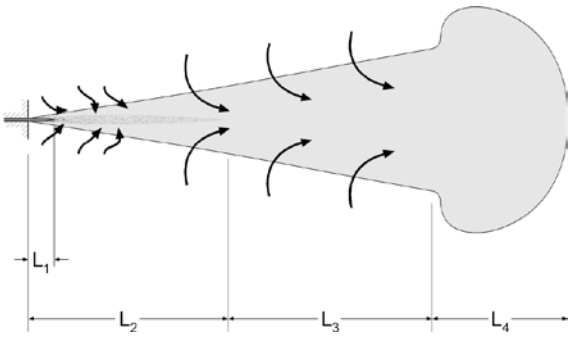

Figure 1. Schematic of a non-reacting full-cone diesel spray

As the vapor jet penetrates into the chamber and mixes with the hot chamber air, chemical reactions occur leading to ignition. Different regimes of fuel chemistry (low, intermediate and high temperature chemistry regimes) exist for hydrocarbons [34-36]. For a hydrocarbon fuel, the chemical pathway to ignition can involve all three chemistry regimes depending on the initial temperature and pressure conditions. Ignition can occur either through a single-stage or a two-stage process depending on the conditions. Once ignition occurs, usually at multiple spots around the vapor jet, flames develop from the ignition kernels and connect to form a highly-wrinkled flame surrounding the jet. Figure 2 is a schematic showing the reacting diesel spray [35, 37]. Representative values of temperature, and various reaction regimes, are indicated on the figure. Westbrook [35] associated the different regions in the reacting spray with different hydrocarbon chemistry regimes. Downstream of the liquid-phase penetration length, "premixed" phase of combustion occurs in fuel-rich regions. Here, the temperature of the fuel/air mixture is low, and hence, the reaction rate is slow. As more air is entrained, the temperature of the fuel/air mixture increases, and reaction rate increases. Once the temperature of the fuel/air mixture increases above 800 K, low temperature chemical reactions become increasingly important. Formation of meta-stable H_2O_2 then slows down reactions. However, moderate heat release from the low temperature chemistry increases the temperature accelerating the chain-branching decomposition reaction of H_2O_2 to hydroxyl radicals, and thermal runaway then occurs leading to autoignition of the spray. Nitric oxide forms on the lean side of the flame where the oxygen concentration and temperature are optimum. It has been postulated that soot precursors start forming in the rich premixed fuel/air mixture and they are transported downstream where they form soot particles. The maximum concentration of soot particles has been suggested to be in the head vortex of the transient jet [37]. As indicated in Fig. 2, the flame is lifted from the base and the lift-off height has been correlated with the soot formed in the jet.

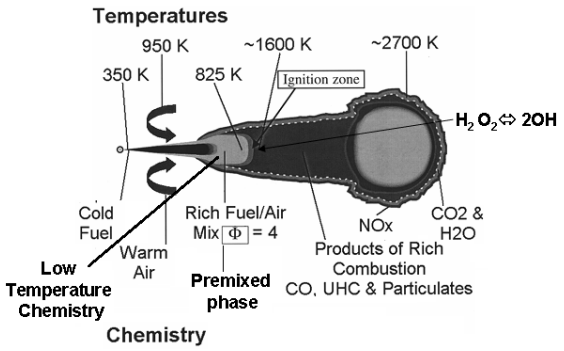

Figure 2. Conceptual picture of a combusting diesel-jet [35, 37].

Siebers and Higgins [38] experimentally investigated the effects of various parameters such as injection pressure, ambient gas temperature and density on the lift-off height. They concluded that the lift-off height is inversely related to the ambient temperature and ambient density whereas it is directly related to the injection pressure. Siebers *et al.* [39] extended these studies to consider the effect of ambient oxygen concentration on the lift-off height. They concluded that the lift-off height was inversely related to oxygen concentration. Later, Pickett *et al.*, [40] showed a dependence of the lift-off height on the orifice diameter and also on ignition characteristics. While these studies have been in constant-volume chambers, Persson et al. [41] employed several fuels to study fuel effects on autoignition and flame lift-off in an-optically accessible

engine. They concluded that lift-off height has a weak dependence on ignition delay. A power-scaling law has been proposed to fit the experimental data for the lift-off heights in diesel jets for wide range of conditions [38, 39]. It is given as

$$L_F \sim (\Delta P_{inj})^{0.5} (T_{ambinet})^{-3.74} (\rho_a)^{-0.85} (O_2)^{-1.0} \quad . \tag{1}$$

ΔP_{inj} is the difference in pressure across the orifice, and $T_{ambinet}$, ρ_a and O_2 are ambient temperature, density and oxygen concentration, respectively.

The review below focuses on the capability of multidimensional spray models to predict the structure that we have summarized above. In the next section, we will focus first on the non-reacting spray and then the reacting spray. Section 3 will highlight the limitations of current models and conclude the review.

2. Predictive capability of multidimensional spray models

2.1 The non-reacting diesel spray

An essential point to take into consideration when modeling high-pressure diesel sprays in high-pressure, high-temperature chambers is that the vaporization of the drops is mixing-controlled, i.e. the rate of vaporization is controlled entirely by the rate at which hot air is entrained [7, 15, 21-22, 42]. In other words, the drop size is not limiting vaporization. This suggests that either a spray model with drops or a vapor jet model with the same mass and momentum flow rate as the spray can predict the non-reacting diesel spray accurately. That this can be done has been unequivocally shown in several references [7, 15, 42]. In using a vapor jet model to represent the spray, the assumption is that turbulent jets of the same mass and momentum flow rates have similar structure, i.e. spreading and penetration rates [7, 13, 23, 24, 42]. In the model, the diameter, injection density, and injection velocity of the vapor jet are obtained by equating the mass and momentum flow rates of the liquid spray with the vapor jet. Equating the mass flow rates of the spray and gas jet gives

$$\rho_g V_g A_g = \rho_l V_l A_l \quad , \tag{2}$$

where, ρ_g, ρ_I are the gas and liquid densities respectively, V_g and V_I are the gas and liquid injection velocities and A_g and A_I are the gas and liquid orifice areas. Equating the momentum flow rates gives

$$\rho_g V_g^2 A_g = \rho_l V_l^2 A_l \quad . \tag{3}$$

Dividing (3) by (2) we obtain

$$V_g = V_l \quad . \tag{4}$$

Hence the injection velocity of the vapor jet is the same as that of the measured spray. Substituting (4) in (2) and rearranging

$$A_g = \frac{\rho_l}{\rho_g} A_l \quad , \tag{5}$$

or

$$d_g = \left(\frac{\rho_l}{\rho_g} \right)^{0.5} d_l \quad , \tag{6}$$

where d_g = orifice diameter for vapor injection and d_l= orifice diameter for liquid injection. Note that the equations above make the assumption that the pressure at the injector orifice is equal to the pressure in the chamber [42, 43].

Figure 3 shows measured and computed images of the vapor fuel in a diesel spray [7]. The measured images were obtained at Sandia National Laboratories (www.sandia.gov/ecn) and show ensemble-averaged two-dimensional Rayleigh-scattering images [44]. The computed images were obtained in three ways: through a spray computation, through a vapor jet computation, and a third through a vapor jet injection in which a line source (the virtual liquid source, VLS) was employed for mass, momentum and energy transfer. In the spray model, the liquid phase is treated as a dispersed phase in a continuum of gas [11, 45-47], i.e. the Lagrangian drops Eulerian Fluid (LDEF) approach. The experimental and computational conditions are given in Table 1. The orifice diameter of 0.0927 mm used in the computations includes the effect of the area contraction coefficient. In the liquid spray computation, drops were injected from a line source whose length for the conditions of this work is selected to be 4.6 mm [1], half the liquid penetration length. Varying the source length by +/- 25% did not noticeably influence the results. The drops are injected within an included angle of about 14 degrees. Collisions and secondary breakup are modeled [11, 46]. Figure 3 shows that there is qualitative agreement between the computed and measured images.

Table 1. Experimental and computational conditions

	Experiment	**LDEF**	**VLS**	**Gas jet**
Ambient temperature (K)	1000	1000	1000	1000
Ambient density (kg/m^3)	14.8	14.8	14.8	14.8
Injection pressure (MPa)	150			
Injected fluid	n-heptane	n-heptane	n-heptane	n-heptane
Density of injected fuel (kg/m^3)		630	630	136.9
Velocity coefficient	0.93			
Injection velocity (m/s)		632.4	632.4	632.4
Injected fluid temperature (K)	373	373	373	373
Area contraction coefficient	0.86			
Orifice diameter (mm)	0.100	0.0927	0.0927	0.199
Liquid length (mm)	9.5		9.2	

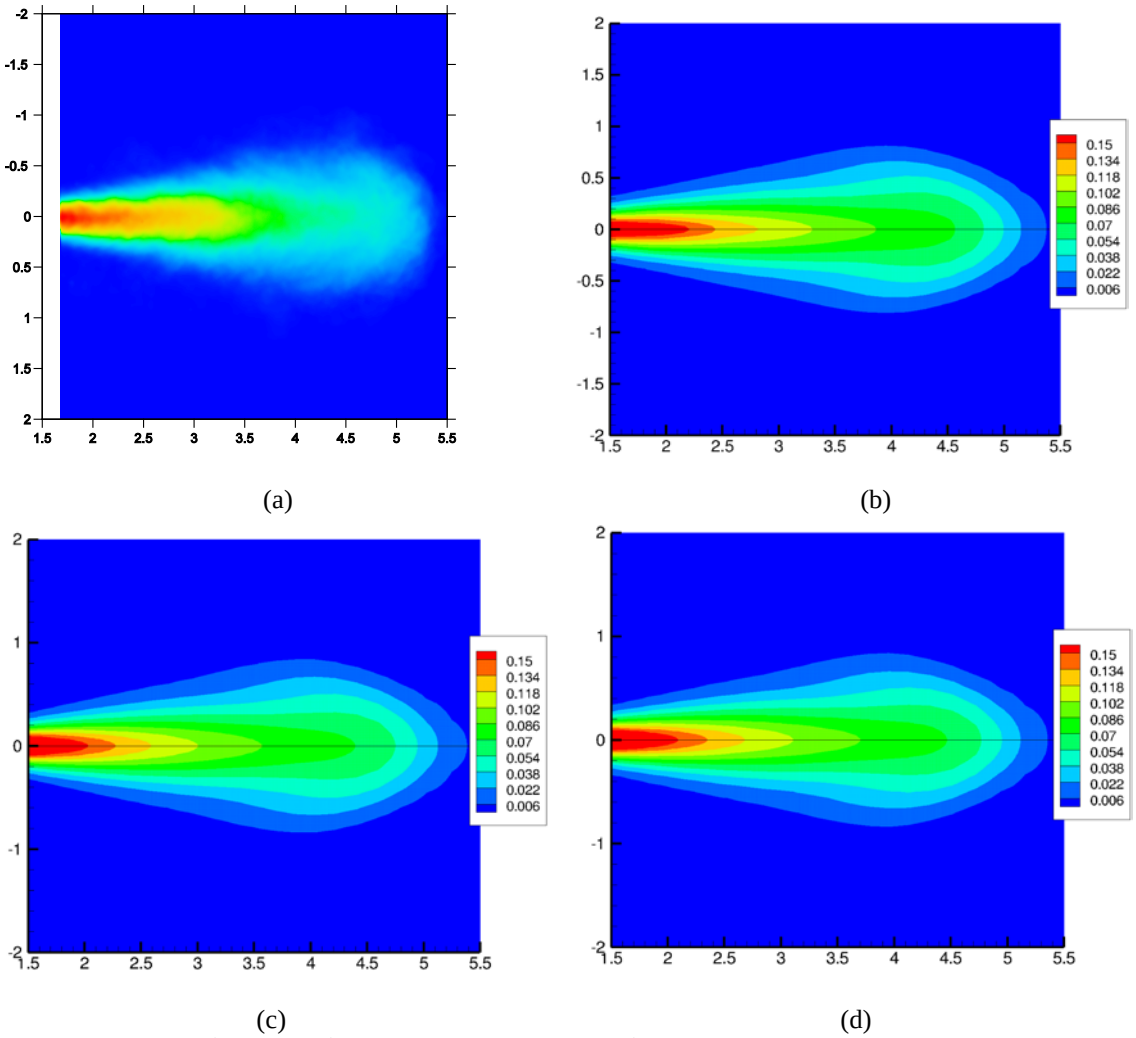

Figure 3. Measured image of the mixture fraction (a), and computed mixture fraction contours at 1.13 ms ASI with the (b) spray, (c) VLS, and (d) gas jet models. Color legend identifies values of mixture fraction.

Figure 4 (a) shows the measured and computed axial centerline mixture fraction (vapor fuel fraction) 0.90ms ASI. The shading on the measured trace indicates the uncertainty band. Beyond about 1.5 cm from the orifice, when all the liquid fuel vaporizes, the differences in computed results are small. The leading edge of the measured spray shows a steeper slope relative to the computed sprays. Figure 4 (b) shows the radial distribution of mixture fraction at an axial distance of 20 mm at 6 ms ASI. The radial spreading of the computed jets is greater relative to the measurements. Since the three (different) models predict very similar results, the differences at the leading edge and in vapor fraction values along the centerline arise from the basic Reynolds-averaged modeling approach. The k-e model is known to overpredict the spreading by about 30%, and the leading edge is smeared by the model [48, 49]. Additional results and discussion are provided in Ref. [7]. An important point to note is that the differences between the computed and measured results are greater during the transient phase.

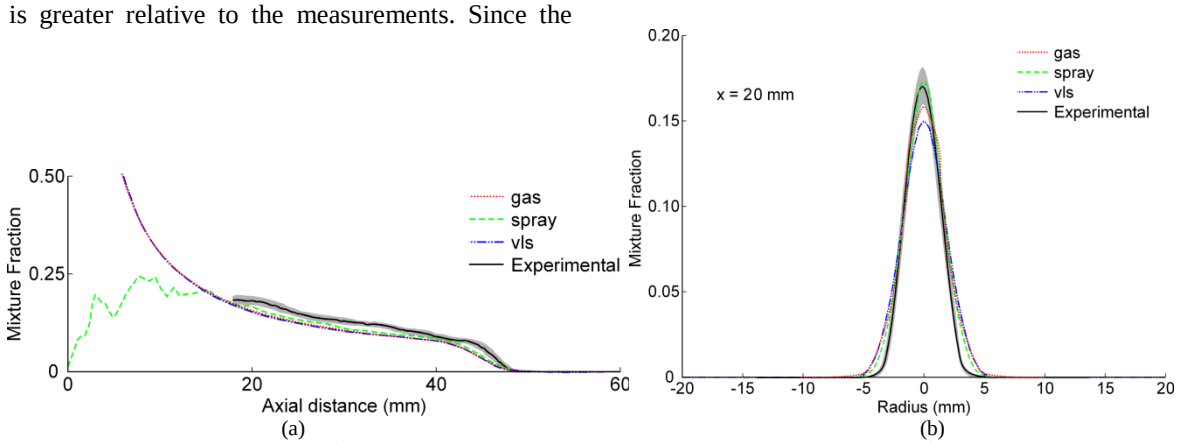

Figure 4. Computed and measured mixture fraction along (a) jet centerline at 0.9 ms ASI, and (b) at axial plane of 20 mm at 6 ms ASI.

The gas jet behavior of the diesel spray is also shown in Fig. 5 (a) which shows the computed penetration of the same diesel spray injected into a chamber with different densities. Figure 5 also shows the corresponding theoretical penetration (shown by dotted lines) obtained using incompressible gas jet theory employing the following expression for tip penetration x_{tip} [14, 23]:

$$x_{tip}^2 = \frac{2(0.4)3d(\rho_l/\rho_a)^{0.5}U_i t}{16\pi^{0.5}C_t}, \qquad (7)$$

where C_t is a constant of value 0.0146.

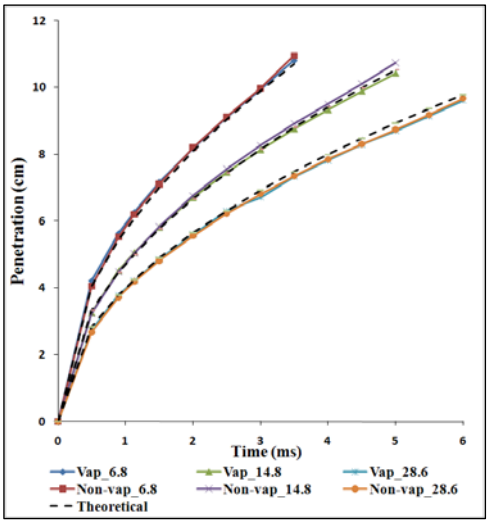

(a)

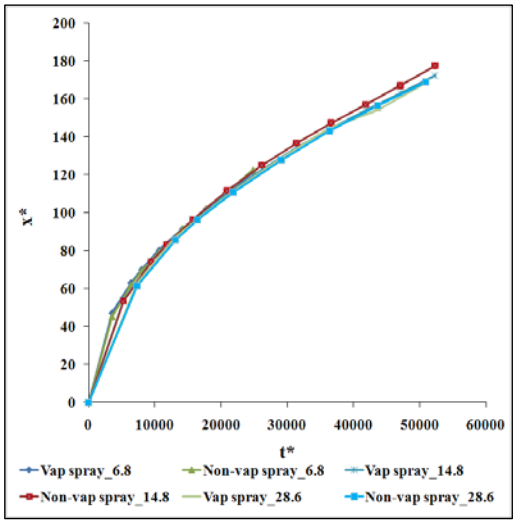

(b)

Figure 5: Equivalence of diesel sprays and gas jets. (a) Penetrations of vaporizing and non-vaporizing sprays, (b) Non-dimensional penetration vs time

In fact, the equivalence of these sprays and a gas jet can be shown by non-dimensionalizing variables as follows [42]:

$$x^* = \frac{x}{(d)\left(\sqrt{\frac{\rho_i}{\rho_a}}\right)}, \qquad (8)$$

$$t^* = \frac{(t)(U_i)}{(d)\left(\sqrt{\frac{\rho_i}{\rho_a}}\right)}, \qquad (9)$$

where, x is the axial distance, t is the time ASI, d is the injector orifice diameter, ρ_i is the injected liquid density, ρ_a is the ambient density, U_i is the injection velocity, and the variables with asterisk are non-dimensional. Figure 5 (b) shows the non-dimensional penetration as a function of non-dimensional time. Not surprisingly, all the lines collapse.

In the computations, the drop size, its distribution, length of the line source, and the angle, are all parameters which are not known. For the results shown, the Sauter mean diameter (SMD) of the drop was assumed to be 2 μm. This SMD was selected to give a liquid-phase length that is consistent with the measured value, i.e. approximately 9 mm. Larger drop sizes result in longer liquid-phase length and larger differences between computed and measured results. Smaller drop sizes do not generally influence the results. The choice of the unknown parameters are all based on various assumptions, which cannot be assessed under conditions of interest because of the absence of relevant experimental data, e.g. drop sizes and size distribution, within the first 50 diameters of the spray. While this is not a severe constraint in diesel sprays, it is a constraint in injection at lower pressures into engines where the liquid phase plays a more dominant role in the behavior of the spray.

The challenges in modeling non-reacting sprays are compounded by the fact that the Lagrangian drop Eulerian gas approach is valid only when the liquid volume fraction is fairly small (less than 1%) in computational cells, and when the drops are homogeneously distributed in the computational space, neither of which is satisfied in the near-field of the spray. To keep the liquid volume fraction small, and ensure numerical stability, computational cell sizes which are larger than the orifice diameter are typically employed. These grid sizes are not adequate to resolve the shear layer, and, not surprisingly, lead to results that are often inaccurate. Alternate approaches that are numerically more accurate, but which still require atomization and drop interaction sub-models, have been proposed [18, 19], but are computationally more intensive. For the computations described above with the spray model, the grid size stretches in the radial direction from 0.3 mm at the injector to 2 mm at the wall. In the axial direction, it stretches from 0.25 mm at the injector to 4.8 mm. The choice of this grid resolution is not dictated by accuracy but by the need to maintain a small liquid volume fraction in the computational cells near the orifice. With this choice of grid, the volume fraction is less than 3%. For the vapor jet simulations, there are 4 numerical cells within the orifice radius, and outside the orifice the grid stretches from 0.08 mm to 3 mm in the radial direction, and 0.25 mm to 4.8 mm in the axial direction. In the case

of the vapor jet, higher resolutions were employed in additional computations to ensure that the results presented here are insensitive to grid resolution. It is not possible to ensure this in the case of the spray computations. In general, the inaccuracies as a result of inadequate resolution are greatest during the transient phase. A point worth noting is that Lagrangian computations are generally less diffusive (from a numerical perspective) compared to Eulerian computations. This suggests that the spray simulations may not need as fine a resolution as the vapor jet simulation, and this may explain why the spray simulations are reasonably accurate in the computations described above. An important point to take away from this discussion is that the high resolutions required to achieve grid independence in diesel jet simulations are generally impractical for engine applications and special gridding strategies have to be employed.

2.2 The reacting diesel spray

It is interesting to consider how the modeling of *reacting* diesel sprays has evolved. In the 1970s and 80s, prior to emissions regulations arising as a major consideration in diesel engine design, it was understood that once ignition has occurred, the heat release in the engine was primarily mixing-controlled. As a result, a combination of a kinetic model for ignition (often using artificial species as in the Shell model of Halstead et al. [50], or even simpler model [51]) coupled with a mixing-controlled model for subsequent diffusion combustion was successfully employed to predict diesel combustion and diesel-engine pressures [52-55]. The need for including chemical kinetics has arisen because of the need to predict ignition, flame lift-off, and (most importantly) pollutants more accurately as reducing emissions has become critical in diesel engine design within the last 20 years. The complexity of the chemical kinetics required depends on the specific objectives of the computation.

Consider the prediction of ignition delay, i.e. the time from start of injection to the occurrence of ignition. It affects thermal efficiency and the NO_x and hydrocarbon emissions. During the ignition delay period, the liquid fuel is atomized, it vaporizes and mixes with the surrounding gases and low-temperature chemical reactions occur. The ignition delay is usually defined based on the time taken to attain a set temperature, the time taken for a rate-controlling radical, such as OH, to reach a set value, or related to the rise in pressure in the chamber. Modeling of ignition within the context of detailed multidimensional computations typically requires the use of multistep chemical reaction mechanisms. The mechanism may involve artificial species, as in the Shell model [50], and reaction steps curve-fitted to match experimental results. These pseudo-mechanisms, however, lack generality. The more realistic approach is to employ multistep kinetics for surrogate fuel species. Detailed chemical-kinetic mechanisms for low-, intermediate-, and high-temperature n-heptane oxidation are available [34] and several models exist that have sufficiently reduced dimensionality (number of species and reactions) to enable their use in CFD simulations [56, 57].

Recently, Bajaj et al. [58] carried out a detailed set of simulations of n-heptane sprays and compared, measured, and computed ignition delays by employing two reduced mechanisms, a 37-species mechanism proposed by Peters et al. [57] and a 44-species mechanism proposed by Liu et al. [36]. N-Heptane has often been used as a surrogate for diesel fuel. It is attractive because of the availability of detailed chemical mechanisms. Higher-order hydrocarbons are, however, becoming better characterized and may be more suitable for future work. The measurements were obtained at Sandia National Laboratories (www.sandia.gov/ecn/) and the experimental conditions are listed in Table 2 and the computed and measured ignition delays using the 44-species mechanism are listed in Table 3. The computations were carried out with a RANS model. The disagreement is greatest for the cases with reduced oxygen concentration and increased chamber density. These differences may arise from inadequacies in the reduced kinetic model and/or from the turbulence/chemistry interaction model. The turbulence/chemistry interaction model will be discussed next.

Table 2. Computational conditions.

Case	d_{noz} (mm)	d_{gas} (mm)	P_{inj} (MPa)	P_{amb} (bar)	T_{fuel} (K)	$T_{ambient}$ (K)	$\rho_{ambient}$ (kg/m^3)	O_2%
1	0.1	0.199	150	42.66	373	1000	14.8	21
2	0.1	0.199	60	42.66	373	1000	14.8	21
3	0.1	0.1745	150	55.45	373	1300	14.8	21
4	0.1	0.2097	150	38.39	373	900	14.8	21
5	0.1	0.199	150	43.02	373	1000	14.8	15
6	0.1	0.199	150	43.2	373	1000	14.8	12
7	0.1	0.199	150	43.45	373	1000	14.8	8
8	0.18	0.3858	140	42.66	373	1000	14.8	21
9	0.1	0.1397	150	86.47	373	1000	30.0	15

Table 3. Computed and measured ignition delay.

Case	Ignition Delay τ_{id} (ms)				
	Experimental	Computed Temperature		% difference	
		T_1500	T_2000	T_1500	T_2000
1	0.53	0.542	0.55	2.264	3.773
2	-	0.615	0.63	----	----
3	0.26	0.209	0.213	19.615	18.076
4	0.79	0.898	0.91	13.670	15.189
5	0.73	0.56	0.593	23.287	18.767
6	0.947	1.225	1.26	28.827	33.051
7	1.52	2.17	----	42.763	----
8	0.57	0.65	0.662	14.035	16.140
9	0.38	0.175	0.22	53.947	42.105

2.2.1 Modeling of turbulence-chemistry interaction

The influence of turbulence on the flame is to wrinkle it. In regions of high turbulence intensity, the flame may be extinguished. Turbulent transport can certainly slow down reactions as heat and radicals are transported at rates much greater than in laminar flames. These effects can be captured in direct numerical simulations (DNS). The thickness of the flame in the diesel jet is, however, smaller than the grid size in RANS and large-eddy simulations (LES). As a result, a turbulence-chemistry interaction model is required to account for the effect of the turbulence on the chemistry and vice versa. Early turbulent combustion models employed for engine applications involved a single-step global reaction model with the effect of turbulence modeled using empirical expressions whereby the reaction time scale was assumed to be a combination of a turbulent time scale and a kinetic time scale. The eddy-breakup model [59, 60] assumes a one-step reaction where the fuel or reactive species and oxidizer react at a rate determined by the rate-determining species among the fuel, oxidizer and the major product, e.g. CO_2. This model further assumes that the turbulent reaction rate is directly proportional to the inverse of the turbulent time scale, i.e. the mixing time scale, and the concentrations of the reacting species. One difficulty with the application of such models is the presence of empirical constants which are generally not known á priori in cases of incomplete combustion. Abraham et al. [61] extended this model by using an approach whereby the species concentrations were assumed to change their concentrations such that the change drove the species toward the local equilibrium concentrations in a characteristic time, i.e. the mean reaction rate of each species due to the combined effect of turbulence and chemistry is given by

$$\frac{dY_m}{dt} = -\frac{Y_m - Y_m^*}{\tau_c} \quad , \qquad (10)$$

where Y_m is the mass fraction of species *m*, Y_m^* is the local thermodynamic equilibrium value of the mass fraction, and τ_c is the characteristic time for the achievement of equilibrium. The characteristic time τ_c is assumed to be a combination of a laminar timescale and a turbulent timescale, such that the longer of the two times scales controls the combustion rate. The laminar timescale is of Arrhenius form, and the turbulent timescale is assumed to be proportional to the eddy turnover time ε/k, similar to the approach adopted in Refs. [59, 60].

The partially-stirred reactor (PaSR) model, along with reduced chemical kinetics, has been employed to model turbulence/chemistry interactions in reacting diesel sprays [62–64]. In this model, each computational cell was assumed to be composed of a reacting element and a non-reacting element. The volume fraction of the reacting element was determined from the ratio of the reaction time scale and the turbulence time scale. In fact, a perfectly-stirred reactor (PSR) model with detailed chemical kinetics in each computational cell has also been employed to study the spray liquid length and lift-off height for reacting diesel sprays and the computed results reported to be in good quantitative agreement with the experimental results [65]. The results from this study suggest that at the lift-off height, the combustion is kinetics-controlled and premixed (hence, the justification for using PSR). This model suffered from the requirement of large computational overhead due to the use of detailed kinetics and high resolution. Furthermore, the effect of turbulence-chemistry interaction is not directly captured in this approach.

Marble and Broadwell [66] formulated the coherent flamelet model (CFM) which considers the flow field to be composed of multiple laminar flamelets stretched by the turbulent flow. In this model, the mean reaction rate is obtained as the product of the flame surface density (which is the flamelet area per unit volume) and the local strained laminar flame speed. A transport equation for the flame surface density, measuring the available flame surface area per unit volume, is employed. The mean burning rate is expressed as the product of the flame surface density by the reaction rate per unit flame surface, estimated from laminar flame computations. In fact, the CFM model has evolved into the flame surface density (FSD) model [67, 68]. The FSD model has been

employed to study the transient combustion process from ignition to flame stabilization in diesel jets [69]. As ignition is a transient process between pure mixing and a well-established diffusion flame, a progress variable was introduced in the model. This modeling approach was coupled to a mixing model and a chemistry model, based on the unsteady flamelet equations, which were solved á priori to generate a flamelet database. Although this model is attractive, the implementation is more difficult than the CTC/LECT, PaSR and PSR models.

The conditional moment closure (CMC) model has also been employed for reacting diesel spray simulations and computed and measured results compared [70-72]. The CMC model was proposed by Klimenko [73] and Bilger [74]. Kim and Pitsch [75] formulated the CMC model for LES. The main hypothesis behind CMC models is that the fluctuations in the scalar quantities of interest can be related to the fluctuations in the mixture fraction field. Based on this idea, transport equations are derived for the reactive scalars which are conditionally averaged with the mixture fraction. Conditional averaging of a variable Y_i is defined as

$$\langle Y_i \,|\, \eta \rangle = \langle Y_i \,|\, Z = Z^* \rangle = \frac{P(Y_i)}{P(Z = Z^*)} \,. \qquad (11)$$

In the above equation, Z^* is a particular value of the mixture fraction Z and is usually taken to be the stoichiometric value Z_{st}. The transport equation for the conditionally averaged mass fraction of species *i* is given by

$$\frac{\partial \langle Y_i \,|\, \eta \rangle}{\partial t} + \langle \mathbf{v} \,|\, \eta \rangle \cdot \nabla \langle Y_i \,|\, \eta \rangle - \frac{1}{2} \langle \chi \,|\, \eta \rangle \frac{\partial^2 \langle Y_i \,|\, \eta \rangle}{\partial \eta^2} = \langle W_i \,|\, \eta \rangle \,, \qquad (12)$$

where **v** is the velocity and W_i is the source term for species *i*. Since this equation is being solved for the conditional averages, the only unclosed term in the equation is the conditionally-averaged source term. Similar equations are derived for momentum and enthalpy. Klimenko and Bilger [76] show that the following approximation can be made with negligible errors:

$$\langle W_i(Y_i, h) \,|\, \eta \rangle \approx \langle W_i(Q_i, Q_h) \,|\, \eta \rangle = W_i(Q_i, Q_h) \,, \qquad (13)$$

where $Q_i = \langle Y_i \,|\, \eta \rangle$ and $Q_h = \langle h \,|\, \eta \rangle$. Here, h represents the enthalpy of the mixture. This conditional averaging makes the modeling of the averaged source term considerably easier as no closure models are required. Bilger *et al*. [77] discuss that in applying the CMC model in LES of practical configurations, several challenges still exist like computational feasibility and prescribing the correct boundary conditions.

Another class of models is one where, like the CFM and FSD models, the assumption is made that the diesel combustion occurs through strained flamelets. The unsteady flamelet model was employed to model diesel combustion and emissions first by Pitsch et al. [78]. In their approach, in addition to the conservation equations that are usually solved, equations for the evolution of the flamelet and a transport equation for the variance of the mixture fraction were solved. The unsteady flamelet equations can be written as

$$\frac{\partial \boldsymbol{\varphi}}{\partial t} = \frac{\chi}{2} \frac{\partial^2 \boldsymbol{\varphi}}{\partial Z^2} + \dot{\boldsymbol{\omega}}_{\varphi} \,, \qquad (14)$$

where $\boldsymbol{\varphi}$ is a vector that represents the collective set of all reactive scalars, i.e. temperature and mass fractions of the different species, and $\dot{\boldsymbol{\omega}}_{\varphi}$ represents the corresponding source terms, and χ is the scalar dissipation rate which is, in general, a function of Z. In the RANS and LES computations, the following equations for mixture fraction $\tilde{Z}$ and the variance of the mixture fraction $\tilde{Z}^2$ are solved:

$$\frac{\partial \bar{\rho} \tilde{Z}}{\partial t} + \nabla \cdot \left(\bar{\rho} \tilde{u} \tilde{Z} \right) = \nabla \cdot \left[\frac{\mu_t}{Sc_{\tilde{Z}}} \nabla \tilde{Z} \right] \qquad (15)$$

$$\frac{\partial \bar{\rho} \widetilde{Z''^2}}{\partial t} + \nabla \cdot \left(\bar{\rho} \tilde{u} \widetilde{Z''^2} \right) = \nabla \cdot \left[\frac{\mu_t}{Sc_{\widetilde{Z''^2}}} \nabla \widetilde{Z''^2} \right] + \frac{2\mu_t}{Sc_{\widetilde{Z''^2}}} \left(\nabla \tilde{Z} \right)^2 - \bar{\rho} \tilde{\chi} \qquad (16)$$

The Schmidt numbers have a value of 0.9 in Ref. [78]. The instantaneous *average* value of scalar dissipation rate $\tilde{\chi}$ in a computational cell is obtained in the RANS simulations as [78, 79]

$$\tilde{\chi} = C_{\chi} \frac{\varepsilon}{k} \widetilde{Z''^2} \,. \qquad (17)$$

C_{χ} is a model constant. Equation (17) was employed to compute χ which was assumed to have an error-function profile dependence on Z. Mean values of χ for the entire domain were obtained and employed in Eq. (14) to determine the flamelet solutions which were then employed to determined species and temperature profiles. The use of just one representative flamelet, however, is not adequate to represent certain features of the reacting diesel jet, e.g. the lift-off height.

Venugopal and Abraham [80] extended the interactive flamelet approach by using multiple flamelets (interactively) and showed that such an approach can predict flame lift-off. Using multiple flamelets is, however, computationally intensive. Meanwhile a computationally less intensive approach had been proposed [81-84] in which all thermochemical quantities are parameterized by mixture fraction, reaction progress parameter, and stoichiometric scalar dissipation rate by the solution of Eq. (14). Bajaj *et al*. [58] employed this unsteady flamelet progress variable (UFPV) model to model reacting diesel jets, including ignition and flame lift-off in diesel jets. This model was employed to obtain the results of Table 3 (shown earlier) for ignition delay. In the model, a presumed PDF closure model was employed to evaluate Fávre-averaged thermochemical quantities. For this a beta-distribution was used for the mixture fraction, and Dirac delta function distributions for the reaction progress parameter and the stoichiometric scalar dissipation rate. These Fávre-

averaged thermochemical quantities were tabulated in UFPV libraries and were used as the turbulent combustion model for the RANS simulations. Table 4 shows predicted and measured lift-off heights (www.sandia.gov/ecn/). The T_1500 criterion identifies the lift-off as the axial distance where the temperature reaches 1500 K. The 0.1% Y_{OH} criterion identifies the lift-off as the axial distance where the hydroxyl mass fraction is 0.1% of its maximum value. The agreement is within 12% for all cases except one. Figure 6 shows computed flooded-contour plots of temperature for the nine cases of Tables 2 identifying the lift-off heights.

The UFPV model has also been extended to predict NO_x and soot distribution in the reacting diesel jets of Table 2. For NO_x predictions, the mechanism from GRI-Mech3.0, and for soot the mechanism of Appel et al. [85] was employed. Tracer particles were employed to track the residence time in the jet [86]. Figure 6 shows the NO_x distribution at 4 ms ASI and Fig. 7 shows the soot distribution at the same time in the nine jets. Quantitative comparisons of peak soot volume fraction are within an order of magnitude although the computed spatial location of the peak soot volume fraction is, in general, upstream of the measured results. Quantitative comparisons of the mass of soot predicted in the reacting sprays show that the computed soot normalized by the injected mass correlate with a non-dimensional lift-off height [87].

Table 4. Computational conditions and results for lift-off height.

Case	Lift-off Height L_F (mm)				
		Computed		% difference	
	Experimental	Temperature T_1500	Y_{OH} 0.1%	T_1500	0.1% Y_{OH}
1	17	18.5	18	8.823	5.882
2	13.5*	15.05	14.8	11.481	9.629
3	7.7	8.05	8.25	4.545	7.142
4	25.5	23.3	22.8	-8.627	-10.588
5	23.2	22.9	22.9	-1.293	-1.293
6	29.2	27.3	----	-6.506	----
7	42.3	52.88	----	25.011	----
8	23.97	25.8	25.31	7.634	5.590
9	11.9	12	12.8	0.840	7.563

* Estimated Value: This value is for diesel fuel injected at 432 K

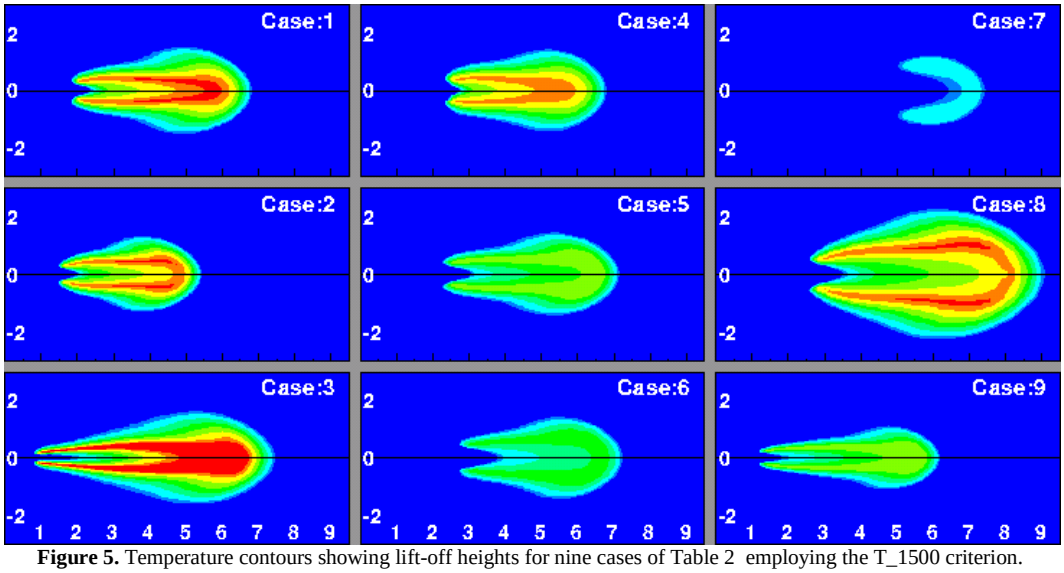

Figure 5. Temperature contours showing lift-off heights for nine cases of Table 2 employing the T_1500 criterion.

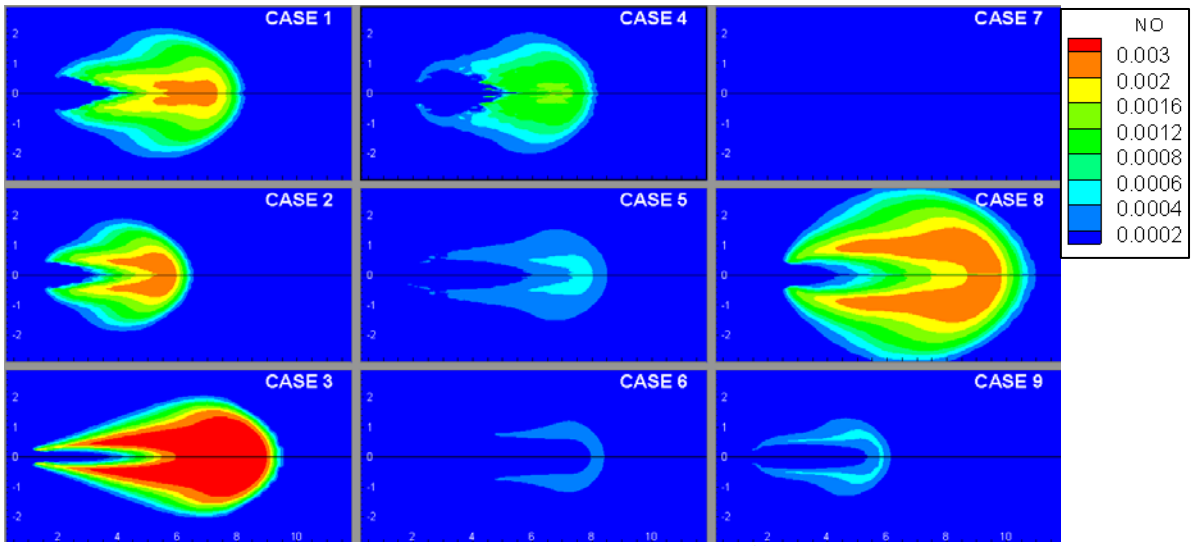

Figure 6. Computed NO distribution in the diesel jets of Table 2.

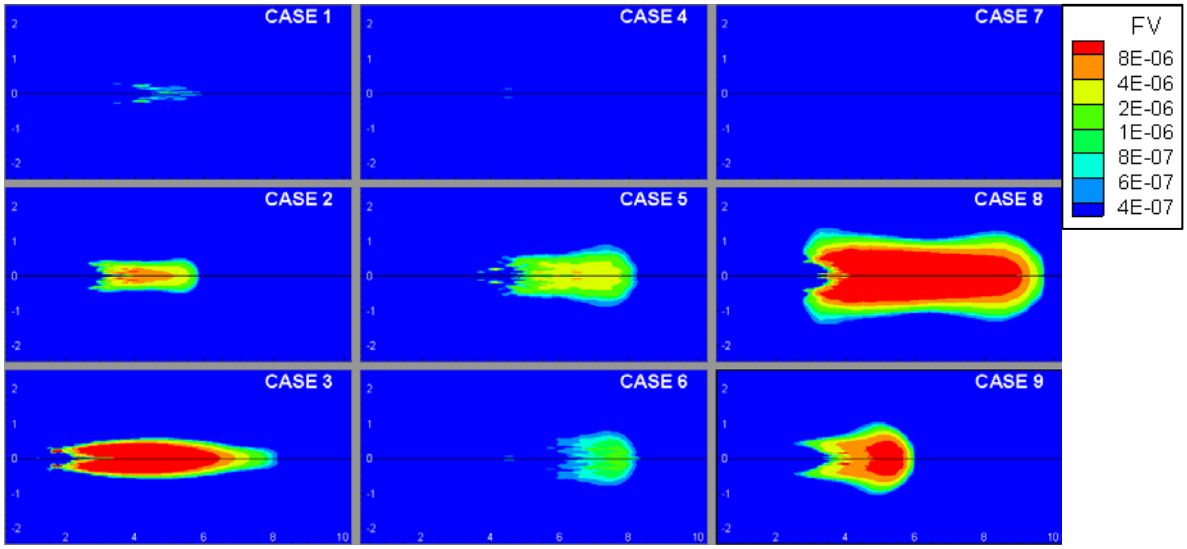

Figure 7. Computed soot distribution in the diesel jets of Table 2.

The major challenge in the application of UFPV model is the selection of appropriate probability density functions (PDF) for the independent scalars and the choice of chemical kinetics. Nevertheless, from this discussion, it can be concluded that if the objective of the simulations is to predict ignition delay and model flame lift-off height, RANS models employing the UFPV model are adequate. In fact, even soot and NO predictions are qualitatively reasonable.

2.2.2 LES of reacting diesel jets

The prediction of soot and NO_x is likely to be dependent on the highly transient nature of the reacting turbulent jet. Furthermore, the transient effects of large scale turbulent structures on lift-off height are likely to influence mixing and subsequently soot and NO_x formation. The RANS models are unable to represent these effects. Diesel combustion is characterized by high chamber pressure and temperature, and high injection Reynolds numbers and consequently small Kolmogorov scales. Thus, the LES of diesel sprays is challenging due to the requirement of very fine grids and small numerical time steps. There have been few LES of non-reacting diesel jets [88-89] and even fewer to reacting diesel jets [90-91]. Hori *et al.* [90] performed LES of reacting diesel jets using the KIVA-LES code. Turbulent combustion was modeled using the eddy-dissipation model. Significant differences were observed in the computed heat release rates when compared to the experimental results. The jet and averaged flame structure was captured reasonably well. The reason for the discrepancy in the heat release rates was attributed to the relatively large grid sizes which were not able to capture all the energy containing scales. In other words, the LES more closely approximated RANS than "true LES". Hu and Rutland [91] applied a flamelet model to represent combustion in their LES of diesel sprays, but this work was primarily in a diesel engine employing a fairly coarse mesh. Recently, Bekdemir *et al.* [92] performed LES of a diesel jet with tabulated chemical kinetics. The tabulated kinetics data was obtained from simulations of laminar igniting counterflow diffusion flames. An unstructured non-uniform grid was used which allowed the presence of fine grid near the nozzle. The ignition delay and flame lift-off heights were in

good agreement with the experimental results. But the unsteady evolution of the flame could not be captured well in their study. Rutland provides a review of LES work in engines which also includes some discussion of sprays [93].

Ameen et al. [94] and Ameen and Abraham [95] have employed LES to study reacting diesel-like jets employing the UFPV model. They studied transient flame evolution from ignition until flame stabilization at the lift-off height and concluded that ignition occurred in multiple spots around the jet and flame stabilized at a location where the scalar dissipation rate was approximately equal to the ignition scalar dissipation rate. The flame lift-off results are consistent with the findings of Bajaj et al. [58]. Figure 8 shows the transient evolution of the flame in the jet.

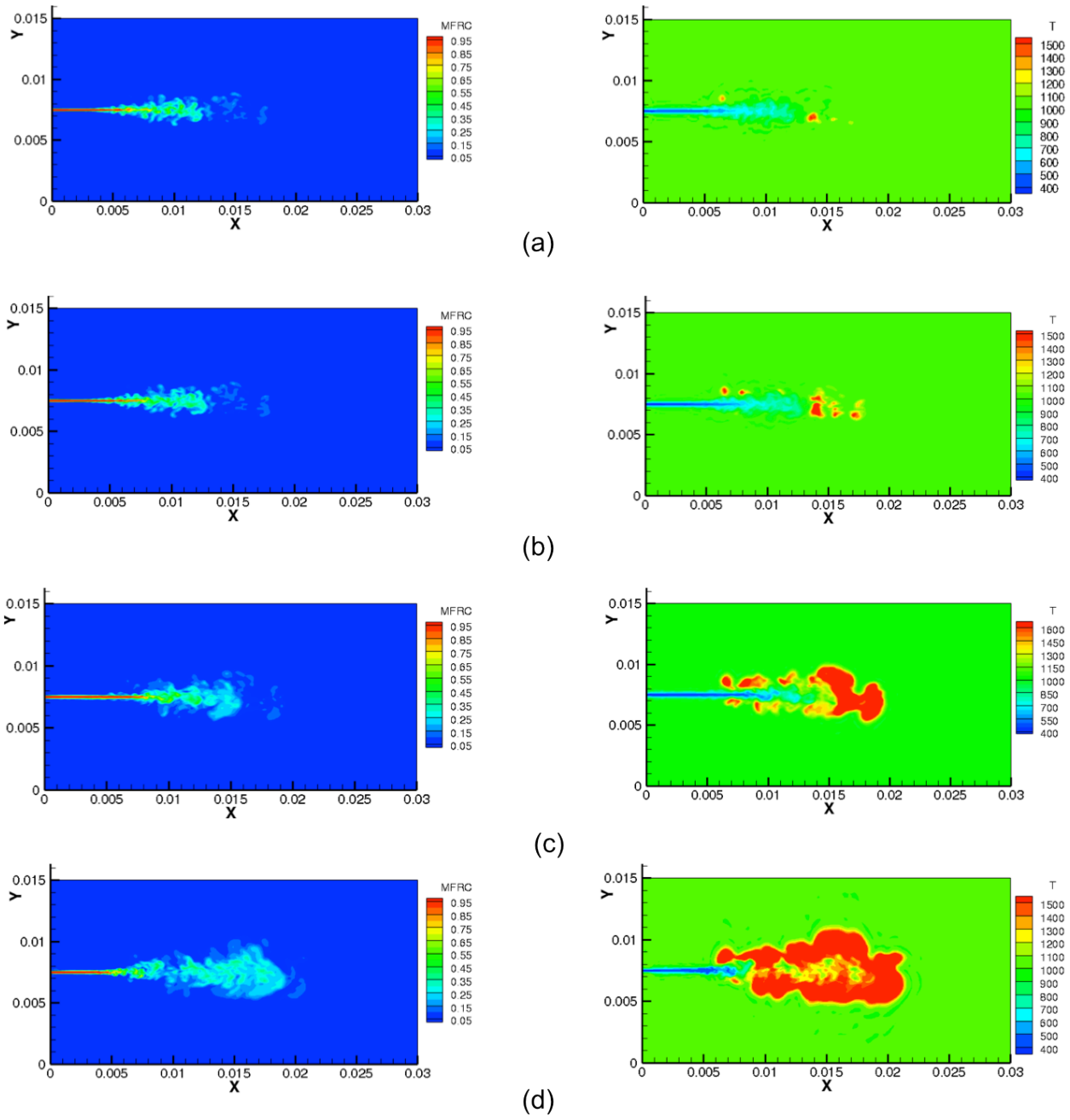

Figure 8. Transient evolution of the mixture fraction (LHS) and temperature (RHS) profiles in the central X-Y plane at (a) 0.32 ms, (b) 0.34 ms, (c) 0.44 ms, (d) 0.60 ms and (e) 0.90 ms ASI.

3. Summary

The discussion in this review will now be summarized with an emphasis on important conclusions and areas of further research. In the case of high-pressure diesel sprays injected into high-pressure high-temperature diesel environments, the vaporization of the liquid phase is mixing-controlled and the penetration of the liquid-phase is relatively short compared to the penetration of the vapor phase. Under these conditions, the spray can be represented as a vapor jet and the quasi-steady part of the jet has properties akin to that of the well-characterized turbulent quasi-steady jet. In fact, it has been suggested that under these conditions, there may be no liquid phase at all because the pressure and temperature in the chamber is supercritical relative to the fuel properties [96], although earlier work has suggested that the supercritical conditions are achieved only if the reduced pressure and temperature are about two [97, 98]. This recent suggestion that the liquid does not exist need further study.

When the fuel injection is into an engine environment under cold-start conditions or into low-pressure low-temperature environment as in low-temperature combustion (LTC) compression-ignition engines, it is important to include the liquid phase. In fact, in these conditions, interaction of the liquid phase with the walls of the chamber may be significant. The accuracy of the atomization (primary, secondary), drop-drop interaction, drop transport, and vaporization models become more critical. Unfortunately, more than thirty years of research into spray atomization notwithstanding, the physics of atomization remains elusive because of the challenges in experimentally characterizing the dense spray regime near the injector orifice. There has been significant progress in numerical simulations of atomization but they involve assumptions about the details of the breakup process. Much work remains to be done. Meanwhile, spray simulations under these conditions will continue to focus on overall spray characteristics such as penetration and spreading.

In the case of reacting diesel sprays, if the only interest is in heat release rates, a hybrid kinetic-mixing controlled model within the context of RANS simulations is adequate. Predicting flame lift-off, however, requires more detailed kinetic representation of the combustion chemistry during the entire period of combustion. It has been shown that representation of the kinetics within the context of perfectly-stirred, partially-stirred reactor, conditional moment closure, flame surface density, and unsteady flamelet progress variable model assumptions are all able to reproduce experimental results with reasonably accuracy in RANS simulations. In other words, the turbulence/chemistry interaction model does not appear to be very critical. This is surprising and more work is needed to understand the reasons.

In the case of engines, injection is intermittent and the spray is inherently transient. There has been no detailed investigation or experimental characterization of the combustion process after the end of injection. Post-injection combustion plays a dominant role in emissions formation/oxidation of hydrocarbons and soot. Additional work is required to understand this phase of combustion in engines.

Nitric oxide in reacting diesel sprays can be predicted within reasonable accuracy based on comparisons with engine exhaust data. Soot predictions are, however, very challenging. When compared with experimental soot distribution in reacting diesel sprays, models can at best predict the measured results within an order of magnitude and distributions often do not match. Much work remains to be done in this area. In this regard, the importance of multi-scale structures and their transient behavior on emissions formation need to understood. In principle, insight can be gained through large-eddy simulations. Application of large-eddy simulations to reacting diesel sprays is still in its early stages and further work is needed.

All things considered, significant progress has been made in the last quarter century and multidimensional engine models are routinely employed by engine industry in engine development work. When coupled with experimental work, they can provide useful insight and significantly reduce development time.

4. Acknowledgement

The author thanks Mr. Muhsin Ameen and Ms. May Yen, Ph.D. students in the School of Mechanical Engineering at Purdue University for their help in preparing this manuscript. The author also thanks Dr. Lyle Pickett at Sandia National Laboratories, Livermore, CA for productive and stimulating interactions over several years, and Professor Vinicio Magi for many years of collaboration on numerical work. Within the last five years, financial support for the author's work on diesel sprays has been provided by Caterpillar, Inc., John Deere and the US Army Research Office. Computational resources have been provided by the US National Institute for Computing (XSEDE), eRSA, SA, and National Computing Infrastructure, Canberra, Australia.

5. References

[1] F.V. Bracco, SAE Technical Paper No. 850394, 1985.

[2] R. Reitz, Atom. Spray Technol. 31 (1987), pp. 309-337.

[3] H. Hiroyasu and M. Arai, SAE Technical Paper No. 900475, 1990.

[4] R. Aneja and J. Abraham, Combust. Sci. Tech. 138 (1998), pp. 315-335.

[5] J.E. Labs and T.E. Parker, Atom. Sprays 13, (2003), pp. 425-442.

[6] J.E. Labs and T.E. Parker, Atom. Sprays 16 (2006), pp. 843-855.

[7] J. Abraham and L.M. Pickett, Atom. Sprays **20** (2010), pp. 241-250.

[8] B. Chehroudi and F. V. Bracco, SAE Technical Paper No. 850126, 1985.

[9] M.J. Andrews, Atom. Sprays 3 (1993), pp. 29-54.

[10] Y. Yue, C. F. Powell, R. Poola, J. Wang and J. Schaller, Atom. Sprays, 11 (2001), pp. 471–490.

[11] P.J. O'Rourke, Collective Drop Effects on Vaporizing Liquid Sprays, Ph.D., Princeton University, Princeton, N.J., 1981.

[12] F.X. Tanner and G. Weisser, SAE Technical Paper No. 980808, 1998.

[13] J. Abraham, SAE Technical Paper No. 970051, 1997.

[14] V. Iyer and J. Abraham, Combust. Sci. Tech., **130** (1997), pp. 315-334.

[15] V. Iyer, S.L. Post and J. Abraham, Proc. Combust. Inst., **28** (2000), pp. 1111-1118.

[16] J. Xin, L. Ricar, and R.D. Reitz, Combust. Sci. Tech., 137 (1998), pp. 171-194.

[17] J.C. Beale and R.D. Reitz, Atom. Sprays, 9 (1999), pp. 623-650.

[18] V. Iyer and J. Abraham, ASME J. Fluids Engng., **125** (2003), pp. 660–669.

[19] V. Iyer and J. Abraham, Atom. Sprays, **15** (2005), pp. 249-269.

[20] J. Naber, and D. L. Siebers, SAE Technical Paper No. 960034, 1996.

[21] D.L. Siebers, SAE Technical Paper No. 980809, 1998.

[22] D.L. Siebers, SAE Technical Paper No. 1999-01-0528, 1999.

[23] J. Abraham, Num. Heat Trans. **30** (1996), pp. 347–364.

[24] Y. Huang, Ph.D. Thesis, Department of Mechanical and Aerospace Engineering, Princeton University, Princeton, NJ, 2000.

[25] R.D. Reitz and F.V. Bracco, SAE Technical Paper No. 790494.

[26] K.-J. Wu, C.-C. Su, R.L. Steinberger, D.A. Santavicca, and F.V. Bracco, ASME J. Fluids Engng. 105 (1983), pp. 406–413.

[27] G. Pawlak, C.M. Cruz, C.M. Bazan, and P.G. Hardy, *Fluid Dyn. Res.*, 39 (2007), pp. 711-730.

[28] I. Iglesias, M. Vera, A. Sanchez, and A. Linan, Phys. Fluids, 17(3) (2005), 038105.

[29] M. Gharib, E. Rambod, and K. Shariff, J. Fluid Mech., 360 (1998), pp. 121-140.

[30] K. Shariff and A. Leonard, Ann. Rev. Fluid Mech. 24 (1992), pp. 235-279.

[31] T. Takagi, T. Okamoto, A. Ohtani and M. Komiyama, *JSME Intl. J.* 31(1) (1988), pp. 119-126.

[32] M. Musculus, T. Lachaux, L. M. Pickett and C.A. Idicheria, SAE Technical Paper No. 2007-01-0907.

[33] M. Musculus, J. Fluid Mech. 638 (2009), pp. 117-140.

[34] H.J. Curran, P. Gaffuri, W.J. Pitz and C.K. Westbrook, Comb. Flame, 114 (1998), pp. 149-177.

[35] C.K. Westbrook, Proc. Comb. Inst. 28 (2000), pp. 1563-1577.

[36] S. Liu, J.C. Hewson, J.H. Chen, and H. Pitsch, Comb. Flame, 137 (2004), pp. 320-339.

[37] J.E. Dec, SAE Technical Paper No. 970873, 1997.

[38] D.L. Siebers and B. S. Higgins, SAE Technical Paper 2001-01-0530, 2001.

[39] D.L. Siebers, B.S. Higgins, and L.M. Pickett, SAE Technical Paper No. 2002-01-0890, 2002.

[40] L.M. Pickett, D.L. Siebers, and C.A. Idicheria, SAE Technical Paper No. 2005-01-3843, 2005.

[41] H. Persson, O. Andersson, and R. Egnell, Comb. Flame, 158 (2011), pp. 91-97.

[42] C. Bajaj, J. Abraham, and L.M. Pickett, Atom. Sprays, **21** (2011), pp. 411–426.

[43] R. Owston, V. Magi, and J. Abraham, SAE Technical Paper No. 2008-01-1041, SAE Intl. J. Engines, 1(1) (2008), pp. 693-712.

[44] C.A. Idicheria and L.M. Pickett, SAE Technical Paper No. 2007-01-0647, 2007.

[45] J.K. Dukowicz, J. Comp. Phys. 35(2) (1980), pp. 229-253.

[46] P.J. O'Rourke and F.V. Bracco, IMechE Publication 1980-9, 1980, pp. 101-116.

[47] A.D. Gosman and E. Ioannides, AIAA Technical Paper No. 81-023, 1981.

[48] D. C. Wilcox, *Turbulence Modeling for CFD*, 3rd ed. DCW Industries Inc., La Canada, CA, 2006, chap. 4.

[49] V. Magi, V. Iyer, and J. Abraham, Num. Heat Trans., **A40** (2001), pp. 317-334.

[50] M.P. Halstead, L.J. Kirsch, A. Prothero, C.P. Quinn, Proc. Royal Soc. A346 (1975), 515-538.

[51] J. Abraham and F.V. Bracco, SAE Technical Paper No. 932656, 1993.

[52] J.C. Dent and P.S. Mehta, SAE Technical Paper No. 811235, 1981.

[53] Z.-X. Hou and J. Abraham, SAE Technical Paper No. 950608, 1995.

[54] M.A. Patterson and R.D. Reitz, SAE Technical Paper No. 980131, 1998.

[55] S.C. Kong, N. Ayoub, and R.D. Reitz, SAE Technical Paper No. 920512, 1992.

[56] R. Seiser, H. Pitsch, K. Seshadri, W.J. Pitz, and H.J. Curran, Proc. Comb. Inst. 28 (2000), pp. 2029-2037.

[57] N. Peters, G. Paczko, R. Seiser and K. Seshadri, Comb. Flame 128 (2002), pp. 38-59.

[58] C.B. Bajaj, M.A. Ameen and J. Abraham, Comb. Sci. Tech., 185 (2013), pp. 454-472.

[59] D.B. Spalding, Comb. Flame, 13 (1971), pp. 649-657.

[60] B.F. Magnussen and B.H. Hjertager, 16th Symp. (Intl.) on Combustion, 1976, pp 719-729.

[61] J. Abraham, F.V. Bracco, and R.D. Reitz, Comb. Flame, 60 (1985), pp. 309-322.

[62] J. Chomiak and A. Karlsson, 26thSymp. (Intl.) on Combustion, 1996, pp. 2557-2564.

[63] F. Tao and J. Chomiak, SAE Technical Paper No. 2002-01-1114, 2002.

[64] F.P. Kärrholm, F. Tao and N. Nordin, SAE Technical Paper No. 2008-01-0961.

[65] P.K. Senecal, E. Pomraning, and K. J. Richards, T. E. Briggs, C. Y. Choi, McDavid R. M. McDavid and M. A. Patterson, SAE Technical Paper No. 2003-01-1043, 2003.

[66] F. E. Marble and E. Broadwell, The coherent flame model for turbulent chemical reactions, Project SQUID Technical Report TRW-9-PU, 1977.

[67] S. Candel, D. Veynante, F. Lacas, E. Maistret, N. Darabiha and T. Poinsot, Coherent flamelet model: applications and recent extensions. Recent Advances in Combustion Modelling, B. Larrouturou ed., World Scientific, Singapore, 1990.

[68] D. Veynante, O. Lacas, P. Boudier, B. Dillies and J. M. Samaniego, The Coherent Flamelet Model for Propulsion Applications, Ft. Belvoir Defense Technical Information Center FEB, 1992.

[69] F.A. Tap, and D. Veynante, Proc. Comb. Inst. 30 (2005), pp. 919-926.

[70] M. Bolla, T. Gudmundsson, Y.M. Wright, SAE Technical Paper No. 2013-01-1618, 2013.

[71] D. France, M. Bolla, Y.M. Wright and K. Boulouchos, SAE Technical Paper No. 2013-24-0016, 2013.

[72] J. Seo, Y. Lee, I. Han, K.Y. Huh, and H. Kim, SAE Technical Paper No. 2008-01-2411, 2008.

[73] A. Y. Klimenko, Conditional Moment Closure and Diffusion in Conserved Scalar Space, ECOLENScientific Research Lab. Paper, Moscow, Russia, 1990.

[74] R.W. Bilger, Phys. Fluids, A5 (1993), pp. 436-444.

[75] S.H. Kim and H. Pitsch, Phys. Fluids, 17 (2005), 105103.

[76] A.Y. Klimenko and R.W. Bilger, Prog. Ener. Combust. Sci., 25 (1999), pp. 595-687.

[77] R.W. Bilger, S.B. Pope, K.N.C. Bray and J.F. Driscoll, Proc. Combust. Inst., 30 (2005), pp. 21-42.

[78] H. Pitsch, H. Barths and N. Peters, SAE Technical Paper No. 962057, 1996.

[79] R. Venugopal and J. Abraham, Comb. Sci. Tech., 179 (2007), pp. 2599-2618.

[80] R. Venugopal and J. Abraham, SAE Technical Paper No. 2007-01-0134, 2007.

[81] C. D. Pierce and P. Moin, J. Fluid Mech. 504 (2004), pp. 73-97.

[82] M. Ihme, C. M. Cha, and H. Pitsch, Proc. Comb. Inst. 30 (2005), pp. 793–800

[83] M. Ihme and H. Pitsch, Phys. Fluids, 20 (2008), 055110

[84] M. Ihme, and Y.C. See, Comb. Flame, 157 (2010), pp. 1850-1862.

[85] J. Appel, H. Bockhorn and M. Frenklach, Comb. Flame, 112 (2000), pp. 122-136.

[86] M. Yen and J. Abraham, Computations of soot and NO in lifted flames under diesel conditions. Submitted to 2014 SAE World Congress.

[87] M. Yen and J. Abraham, Modeling lifted diesel jets: insights into the correlation between flame lift-off height and soot formation. Paper presented at the 8th U.S. National Combustion Meeting, University of Utah, May 20-23, 2013.

[88] T. Hori, T. Kuge, J. Senda and H. Gen Fujimoto, Large eddy simulation of diesel spray structure in constant volume vessel by use of KIVALES. Paper presented at ICLASS2006.

[89] T. Hori, J. Senda, T. Kuge and H. Gen Fujimoto, SAE Technical Paper No. 2006-01-3334, 2006.

[90] T. Hori, J. Senda, T. Kuge and H. Gen Fujimoto, SAE Technical Paper No. 2007-01-0247, 2007.

[91] B. Hu and C.J. Rutland, SAE Technical Paper No. 2006-01-0058, 2006.

[92] C. Bekdemir, L. M. T. Somers, L. P. H. de Goey, J. Tillou and C. Angelberger, Proc. Comb. Inst. 34 (2013), pp. 3067–3074.

[93] C.J. Rutland, Intl. J. Engine Res. 12 (2011), pp. 421-453.

[94] M. Ameen, V. Magi and J. Abraham, Modeling the transient structure of reacting diesel jets using large eddy simulation. Paper presented at the 8th U.S. National Combustion Meeting, University of Utah, May 20-23, 2013.

[95] M. Ameen and J. Abraham, RANS and LES study of lift-off physics in reacting diesel jets. Submitted to 2014 SAE World Congress.

[96] J. Oefelein, D. Dahms and G. Lacaze, SAE Technical Paper No. 2012-01-1258, 2012.

[97] S.D. Givler and J. Abraham, Prog. Energy Combust. Sci., 22 (1996), pp. 1-28.

[98] J. Abraham and S.D. Givler, SAE Technical Paper No. 1999-01-0511, 1999.